

REDUCED THREE-WAVE MODEL TO STUDY THE HARD TRANSITION TO CHAOTIC DYNAMICS IN ALFVEN WAVE-FRONTS

S. A. Elaskar¹ and J. R. Sanmartin²

¹Departamento de Aeronáutica,
Universidad Nacional de Córdoba, CONICET
Av. Velez Sarfield 1611. Córdoba (5000). Argentina.
e-mail: selaskar@efn.uncor.edu

²Escuela Técnica Superior de Ingenieros Aeronáuticos,
Universidad Politécnica de Madrid,
Plaza Cardenal Cisneros 3, Madrid (28040), España.
e-mail: jrs@faia.upm.es

Abstract. *The derivative nonlinear Schrödinger (DNLS) equation, describing propagation of circularly polarized Alfvén waves of finite amplitude in a cold plasma, is truncated to explore the coherent, weakly nonlinear, cubic coupling of three waves near resonance, one wave being linearly unstable and the other waves damped. In a reduced three-wave model (equal damping of daughter waves, three-dimensional flow for two wave amplitudes and one relative phase), no matter how small the growth rate of the unstable wave there exists a parametric domain with the flow exhibiting chaotic dynamics that is absent for zero growth-rate. This hard transition in phase-space behavior occurs for left-hand (LH) polarized waves, paralleling the known fact that only LH time-harmonic solutions of the DNLS equation are modulationally unstable.*

Key words: Plasmas, Alfvén waves, cubic coupling of three waves near resonance, derivative non-linear Schrödinger equation, hard transition to chaos.

1. INTRODUCTION

Nonlinear Alfvén-wave interactions may be present in astrophysical, space and laboratory plasmas, with effects that range from heating to driving of current. A recent space example involves orbiting conductive tethers, which, if in electrical contact with the ionosphere, radiate Alfvén waves.¹ Wave structures (called *Alfvén wings*) attached at or near both tether ends present an Airy-functions behavior if linearly described.² Nonlinear effects, which should appear at the near wave-front, might be affected by the magnetic self-field generated by the very current of the tether.³

In the case of Alfvén waves, some strong nonlinear effects are known to be described by the derivative nonlinear Schrödinger (DNLS) equation,⁴ which admits soliton solutions.⁵ A variety of behaviors allowed by the DNLS equation and its modifications have been analyzed.⁶

Here we show how the DNLS equation may also serve to describe weak non-linear effects represented by the coherent coupling of a few waves, and we explore its complex dynamics. The local, coherent interaction of three waves at or near resonance (3WRI) is an ubiquitous feature of nonlinear mediums. The 3WRI is specially important in both unmagnetized and magnetized plasmas, where dispersive effects can keep nonlinearities weak and electromagnetic waves make coupling to external energy sources easy. The 3WRI has been extensively studied and remains a basic nonlinear paradigm.⁷

The 3WRI evolution for lossless quadratic coupling, with a mode linearly unstable and the two other modes equally damped, is described by a three-dimensional (3D) flow of two wave amplitudes and one relative phase (a *reduced 3-wave* interaction). If damping rates exceed the growth rate Γ of the unstable mode the system is attracted to point-sets of vanishing 3D volume, and its long-time behavior may be chaotic.⁸⁻¹⁰ For small Γ , a consistent analysis of the flow using a multiple time-scales method, led to an 1D chaotic map.¹¹ Actually, the system exhibits a hard transition to complex phase-space dynamics: no matter how small $\Gamma > 0$ there exists a fully developed attractor that is absent at $\Gamma \leq 0$ and is chaotic for some parametric domain; this is example of a broad scenario for chaos also present in the resonant coupling of two oscillators at frequency ratio $2:q$, q integer, with the first oscillator unstable.¹² Also, the hard transition was found to persist when the daughter waves had unequal dampings, the flow then being 4D rather than 3D.^{13,14}

Cubic interaction, corresponding to $q = 2$ (or 1:1 frequency ratio) in the two-oscillator case, allows a variety of coupling structures. A *reduced 3-wave* truncation of the non-linear Schrödinger equation showed chaotic behavior at finite Γ ;¹⁵ a *hard* transition was encountered in a two-oscillator model of a spherical swing.^{12,16}

In the present paper we explore, numerically, weakly nonlinear dynamics in a truncation of the DNLS equation that shows more complex cubic coupling using the *reduced* model (3D model).¹⁷

In Sec. 2 we present the *reduced 3-wave* model of the DNLS equation. In Sec. 3 we analytically determine the $\Gamma = 0$ attractor of the system. In Sec. 4 we derive analytical results

on the small, positive Γ attractor(s). Sec. 5 shows the numerical results. A conclusions are given in Sec. 6.

2. REDUCED 3-WAVE MODEL OF THE DNLS EQUATION

The derivative nonlinear Schrödinger equation describes the evolution of circularly polarized Alfvén waves of finite amplitude propagating along an unperturbed uniform magnetic field in a cold, homogeneous and lossless plasma. The description uses a two-fluid, quasineutral approximation (with electron inertia and current displacement neglected). Taking the unperturbed magnetic field B_0 in the z direction, the DNLS equation reads⁴⁻⁶

$$\frac{\partial \phi}{\partial t} + \frac{\partial}{\partial z} \left[\phi \left(1 + \frac{|\phi|^2}{4} \right) \right] \pm \frac{i}{2} \frac{\partial^2 \phi}{\partial z^2} + \hat{\gamma} \phi = 0, \quad (1)$$

where ϕ , t and z are dimensionless perturbed field and variables,

$$\phi \equiv \frac{B_x \pm i B_y}{B_0}, \quad \omega_{ci} t \rightarrow t, \quad \frac{\omega_{ci}}{V_A} z \rightarrow z, \quad (2)$$

ω_{ci} is the ion cyclotron frequency and V_A is the Alfvén velocity. The upper (lower) sign in Eqs. (1) and (2) corresponds to a left-hand (right-hand) circularly polarized wave propagating in the z direction; $\hat{\gamma}$ would be some appropriate growth/damping linear operator.¹⁵ Equation (1) can be derived under the following ordering scheme for perturbed quantities (n and v_z are plasma density and velocity along the z -axis):

$$\frac{B_x}{B_0} \approx \frac{B_y}{B_0} \approx \sqrt{\frac{n - n_0}{n_0}} \approx \sqrt{\frac{v_z}{V_A}}.$$

To study weakly nonlinear interactions, we consider an approximate solution of Eq. (1) consisting of three traveling waves,

$$\phi = 2 \sum_{j=1}^3 \phi_j(t) e^{i \lambda_j}, \quad \lambda_j = k_j z - \omega_j t, \quad (3)$$

satisfying a resonance condition $2k_1 = k_2 + k_3$. Wave number and frequency of modes are related by the linear (lossless) dispersion relation for circularly polarized Alfvén waves at low wave number, $\omega_j = k_j \mp k_j^2 / 2$.

Both the growth/damping and the nonlinear term in Eq. (1) make the complex amplitudes ϕ_j vary slowly in time. Introducing Eq.(3) in (1) and considering only the k_1 , k_2 and k_3 components one arrives at

$$\dot{\phi}_1 + \gamma_1 \phi_1 + ik_1 \left[\left(|\phi_1|^2 + 2|\phi_2|^2 + 2|\phi_3|^2 \right) \phi_1 + 2\phi_1^* \phi_2 \phi_3 e^{i\nu t} \right] = 0, \quad (5a)$$

$$\dot{\phi}_2 + \gamma_2 \phi_2 + ik_2 \left[\left(2|\phi_1|^2 + |\phi_2|^2 + 2|\phi_3|^2 \right) \phi_2 + \phi_1^2 \phi_3^* e^{-i\nu t} \right] = 0, \quad (5b)$$

$$\dot{\phi}_3 + \gamma_3 \phi_3 + ik_3 \left[\left(2|\phi_1|^2 + 2|\phi_2|^2 + |\phi_3|^2 \right) \phi_3 + \phi_1^2 \phi_2^* e^{-i\nu t} \right] = 0, \quad (5c)$$

where $\dot{\phi}_j$ is $d\phi_j/dt$ and $\nu \equiv 2\omega_1 - \omega_2 - \omega_3$ is a frequency mismatch. We assume that all other components, in particular those involving wave numbers $2k_2 - k_1$, $2k_3 - k_1$, $2k_2 - k_3$, and $2k_3 - k_2$, arising from using (3) in the nonlinear term of Eq.(1), are strongly damped.¹⁵

Setting $\phi_j(t) = a_j(t) \exp[i\psi_j(t)]$ in Eqs. (5a-c) with a_j , ψ_j real, and using the resonance condition, the above three complex equations are reduced to four real equations,

$$\dot{a}_1 = -\gamma_1 a_1 - (k_2 + k_3) a_1 a_2 a_3 \sin\beta \quad (6a)$$

$$\dot{a}_2 = -\gamma_2 a_2 + k_2 a_1^2 a_3 \sin\beta \quad (6b)$$

$$\dot{a}_3 = -\gamma_3 a_3 + k_3 a_1^2 a_2 \sin\beta \quad (6c)$$

$$\dot{\beta} = \nu + \left[a_1^2 \left(k_2 \frac{a_3}{a_2} + k_3 \frac{a_2}{a_3} \right) - 2(k_2 + k_3) a_2 a_3 \right] \cos\beta - k_2 [a_1^2 - a_2^2] - k_3 [a_1^2 - a_3^2] \quad (6d)$$

where $\beta \equiv \pi + \nu t + \psi_2 + \psi_3 - 2\psi_1$.

We restrict the analysis to the case $\gamma_2 = \gamma_3 \equiv \gamma$. Multiplying Eq. (6b) by $2k_3 a_2$, Eq. (6c) by $2k_2 a_3$, and subtracting from each other there results

$$\frac{d}{dt} (k_3 a_2^2 - k_2 a_3^2) = -2\gamma (k_3 a_2^2 - k_2 a_3^2); \quad (7)$$

Eq.(7) shows $k_3 a_2^2 - k_2 a_3^2$ (but not a_2^2 or a_3^2) to decay exponentially with time. For a study of the long time behavior of the system, we may then take $k_3 a_2^2 = k_2 a_3^2$ from the outset. Note that the frequency mismatch is positive and negative for left-hand (LH) and right-hand (RH) polarization respectively: using Eq.(4) one finds in dimensional form

$$\frac{\nu}{\omega_{ci}} \approx \pm \left(\frac{\omega_1}{\omega_{ci}} \right)^2 \left(\frac{k_2 - k_3}{k_2 + k_3} \right)^2. \quad (8)$$

This sign difference will later be shown to lead to fundamentally different dynamics for the two polarizations. Finally we may both take $k_3 < k_2$ and equal signs for a_2 and a_3 with no loss of generality (for opposite signs, setting $\beta \rightarrow \pi + \beta$ would again leave the system invariant); also, we may take all three a_1, a_2, a_3 positive.

Writing $\gamma_1 \equiv -\Gamma < 0$ and introducing new variables

$$\sqrt{k_2 k_3} a_1^2 \rightarrow a_1^2, \quad (k_2 + k_3) \sqrt{k_3 / k_2} a_2^2 \rightarrow a_2^2,$$

system (6a-d) is reduced to three real non-linear equations

$$\dot{a}_1 = \Gamma a_1 - a_1 a_2^2 \sin \beta, \quad (9a)$$

$$\dot{a}_2 = -\gamma a_2 + a_1^2 a_2 \sin \beta, \quad (9b)$$

$$\dot{\beta} = \nu - 2(a_1^2 - a_2^2)(\bar{V} - \cos \beta) - a_2^2 / \bar{V}, \quad (9c)$$

where

$$\bar{V} \equiv \frac{1 + k_3 / k_2}{2\sqrt{k_3 / k_2}} > 1, \quad \left(\frac{k_3}{k_2} < 1 \right). \quad (10)$$

The limit case $\bar{V} = 1$ would exactly recover a truncation of the 1D nonlinear Schrödinger equation describing the parametric excitation of linearly damped waves by the oscillating two-stream instability in plasmas.¹⁵ We also note that some resonant interactions of two oscillators with frequency ratio 1:1, which have been analyzed by López-Rebollal and Sanmartín, are described by system (9a-c) with the last term in (9c) missing.¹²

3. $\Gamma = 0$ ATTRACTOR FOR THE REDUCED 3-WAVE MODEL

In this section we discuss analytical results that can be readily obtained from system (9a-c) and we determine its $\Gamma = 0$ attractor. A trivial result concerns the flow divergence in (3D) phase-space a_1^2, a_2^2 , and β , reading

$$\frac{\partial}{\partial a_1^2} \frac{d a_1^2}{dt} + \frac{\partial}{\partial a_2^2} \frac{d a_2^2}{dt} + \frac{\partial}{\partial \beta} \frac{d \beta}{dt} = 2(\Gamma - \gamma).$$

Nonlinear conservative coupling naturally preserves volume. For $\Gamma < \gamma$, as assumed here, the long-time attractor of the system will be a point-set of vanishing 3D volume.

Again from system (9a-c) one obtains equations that would represent conservation laws in the no-dissipation limit,

$$\frac{d}{dt}(a_1^2 + a_2^2) = 2\Gamma a_1^2 - 2\gamma a_2^2, \tag{11}$$

For $\Gamma < 0$, Eq.(11) proves the equilibrium state $a_1 = a_2 = 0$ to be a global attractor. In this section we consider the long-time attractor of system (9a-c) at $\Gamma = 0$. Note that the entire flow is now asymptotic to the surface $a_2=0$, because $a_1^2 + a_2^2$ will keep diminishing in Eq.(11) unless a_2 vanishes. Since that surface is invariant, trajectories should be asymptotic to its critical elements with transverse stable manifolds.

Consider then the flow on $a_2 = 0$ at $\Gamma = 0$, Eq.(9a) then yielding $a_1 = constant$. The intersection of the plane $a_2 = 0$ and the cylindrical surface $h_0(a_1, \beta) \equiv \beta(a_2 = 0) = 0$ is a line Λ of fixed points,

$$a_2 = 0, \tag{12a}$$

$$h_0 \equiv v - 2 a_1^2 (\bar{V} - \cos\beta) = 0. \tag{12b}$$

Figure 1 shows both Λ and the surface $h_0 = 0$ for $\bar{V} > 1$; Λ would reach up to infinity for $\bar{V} = 1$. Linearizing the vector field at the fixed points we find eigenvalues $\lambda_1 = -2a_1^2 \times \sin\beta$, and $\lambda_2 = 0$, for eigenvectors tangent to the line $a_1 = constant$ through the corresponding fixed point, and tangent to Λ , respectively. From the sign of λ_1 it follows that, for flow on $a_2 = 0$, Λ -points with $\beta < \pi$ are stable and $\beta > \pi$ points are unstable; two $a_1 = constant$ heteroclinic orbits join each symmetric pair of Λ points.

The third eigenvalue is clearly the factor multiplying a_2 in Eq.(9b), $\lambda_3 = -\gamma + a_1^2 \sin\beta$, with the associated eigenvector parallel to the a_2 -axis. It follows that for motion off $a_2 = 0$ the $\beta > \pi$ branch is stable, whereas in the branch $\beta < \pi$, under condition

$$\bar{V}^2 < 1 + (v/2\gamma)^2, \tag{13}$$

there are points P_0 and P_0^* that have $\lambda_3 = 0$ and are given by

$$a_1^2 = \frac{\gamma}{\sin\beta} = \frac{\bar{V} v \mp \sqrt{v^2 - 4\gamma^2(\bar{V}^2 - 1)}}{2(\bar{V}^2 - 1)} \tag{14}$$

for - and + signs respectively, with $\beta(P_0^*) < \pi/2$ always, but $\beta(P_0) > \pi/2$ for $v/2\gamma > \bar{V}$. Only Λ -points in the arc $P_0P_0^*$ are unstable off $a_2 = 0$. For the flow in the entire 3D space

the stable fixed points are those in the $\beta < \pi$ branch of Λ below P_0 and above P_0^* . Note that $a_1(P_0^*) \rightarrow \infty$ as $\bar{V} \rightarrow 1$.

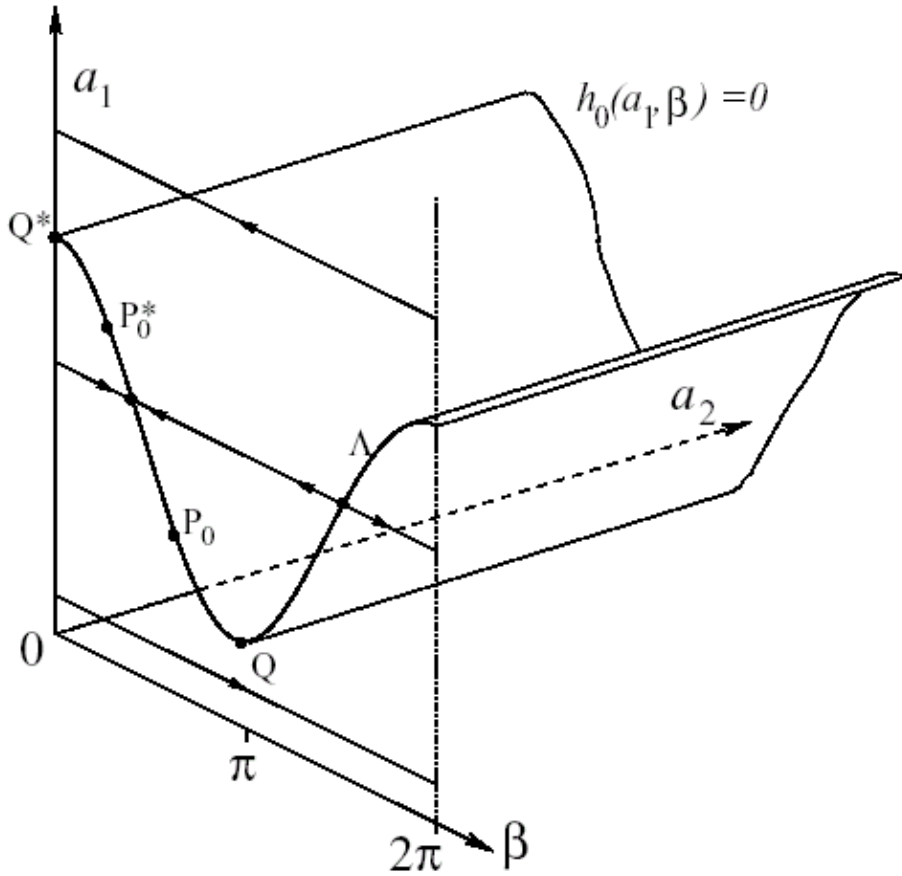


Figure 1. Line Λ of fixed points on invariant plane $a_2 = 0$ at $\Gamma = 0$, and periodic orbits above and below; for $\beta < \pi$ only the arcs QP_0 and $P_0^*Q^*$ are stable off $a_2 = 0$. Also shown is the cylindrical surface $h_0(a_1, \beta) = 0$.

In the plane $a_2 = 0$ there is another type of critical elements. There are periodic orbits that move below the bottom Q of Λ at constant $a_1 < a_{1Q}$, from $\beta = 0$ to $\beta = 2\pi$, and that are described by Eq.(9c) now reading $\dot{\beta} = h_0(a_1, \beta)$; again, there are periodic orbits above Q^* in Fig.1. [Their period is $\pi / [(\bar{V} a_{10}^2 - v/2)^2 - a_{10}^4]^{1/2}$, which diverges for $a_{10} = a_{1Q}$ ($a_{10} = a_{1Q^*}$), when the periodic orbit becomes an homoclinic trajectory at Q (Q^*), as seen in the figure.] Clearly, $a_2 = 0$ perturbations of any such orbits leave the system moving in another nearby orbit. Also, all these periodic orbits are stable off $a_2 = 0$: At vanishing a_2 we have $\dot{\beta} = O(1)$ whereas a_1 changes at a rate of order a_2^2 ; taking $d(\ln a_2)/dt$ from (9b), its average over a period is $-\gamma < 0$, the contribution of the $\sin\beta$ term vanishing.

Under condition (13) one may say that the stable arc QP_0 and the periodic orbits below Q make up one attractor of the flow and the stable arc $P_0^*Q^*$ and the periodic orbits above Q^* make up a second attractor. There is a fundamental difference between these two attractors

however. Since Λ points in the arc $P_0P_0^*$ have an 1D unstable manifold transverse to $a_2 = 0$ there exist singular, heteroclinic orbits that leave this plane at those points, and return to it at a lower a_1 , as seen from Eq.(11) with $\Gamma = 0$. The singular orbit may reach a point in the arc QP_0 from the left, keeping $\beta < \pi$ throughout, or may approach the set of periodic orbits. It may also pass just below the surface $h_0(a_1, \beta) = 0$ to reach the range $\beta > \pi$ still off the plane $a_2 = 0$, making \dot{a}_1 positive in Eq.(9a); the orbit will then emerge at $\beta = 0$ with $a_1 > a_{1Q}$ and again reach a point in the arc QP_0 from the left.

4. $\Gamma \rightarrow 0^+$ ATTRACTOR

When Γ is made positive, there are just two fixed points, P and P^* , given by

$$a_1^2 = \frac{-2\frac{\Gamma}{\gamma}v(2\bar{v} - \bar{v}^{-1}) + 4\bar{v}v \mp 4\sqrt{\frac{\Gamma}{\gamma}[4\gamma^2(4\bar{v} - 5) - 2v^2] + [v^2 - 4\gamma^2(\bar{v}^2 - 1)]}}{8\left[\left(\bar{v}^2 - 1\right) + \frac{\Gamma}{\gamma}\left(3 - 2\bar{v}^2\right)\right]} \quad (15a)$$

$$a_2^2 = \frac{\Gamma a_1^2}{\gamma} \quad (15b)$$

$$\sin\beta = \frac{\gamma}{a_1^2} \quad (15c)$$

under condition

$$\bar{v}^2 < \frac{v^2(\gamma - 2\Gamma) + 4\gamma^2(\gamma - 5\Gamma)}{4\gamma^2(\gamma - 4\Gamma)} \quad (15d)$$

Equation (15a) recovers (14) for P_0 and P_0^* and Eq. (15d) recovers (13) when $\Gamma \rightarrow 0$.

The characteristic equation for the stability of those two points is

$$(\lambda + 2\gamma - 2\Gamma)(\lambda^2 + 4\gamma\Gamma) + \frac{2\gamma\Gamma}{\tan\beta} \left[\frac{\lambda}{\sin\beta} \left\{ \frac{1}{\bar{v}} - 4(\bar{v} - \cos\beta) \right\} - 2v \right] = 0. \quad (16)$$

For $\Gamma = 0$, Eq.(19) again recovers the values $\lambda_1 = -2\gamma$, $\lambda_2 = \lambda_3 = 0$ of Sec. 3. For Γ positive and small, one finds to order $\sqrt{\Gamma}$

$$\lambda_{2,3}(P^*) \approx \pm \sqrt[4]{v^2 - 4\gamma^2(\bar{v}^2 - 1)} \times \sqrt{2\Gamma} \times a_1(P_0^*); \quad (17)$$

P^* at small Γ is thus a saddle-node with an 1D unstable manifold. For the stability of P we must go to order Γ ,

$$\lambda_{2,3}(P) \approx \pm i \sqrt[4]{v^2 - 4\gamma^2(\bar{V}^2 - 1)} \times \sqrt{2\Gamma} \times a_1(P_0) + \bar{\lambda}\Gamma, \quad (18)$$

$$\bar{\lambda} \equiv \frac{1}{2 \tan\beta} \left(\frac{v}{\gamma} - \frac{1}{\bar{V} \sin\beta} \right).$$

The sign of $\bar{\lambda}$ is obtained by taking $\beta(v/\gamma, \bar{V}, \Gamma)$ from Eq.(15a) with the upper sign. We find that P , which only exists under condition (15d) and is defined for $\bar{V} > 1$, is stable above the line $(v/2\gamma)^2 = \bar{V}^2$ [with $\beta(P_0) > \pi/2$ as noticed in Sec. 3] and below the line

$$\left(\frac{v}{2\gamma} \right)^2 = \frac{1}{8\bar{V}^2 - 4\bar{V}^4 - 1}, \quad (\text{for } \bar{V}^2 < \frac{3}{2}) \quad (19)$$

in the parametric plane $(v/2\gamma)^2, \bar{V}^2$. Point P goes through a Hopf bifurcation, $\bar{\lambda}$ becoming positive, when crossing either line. Figure 2 summarizes the stability of P for $\Gamma \rightarrow 0^+$.

Now consider the long-time behavior of the system for Γ very small. Away from the surface $a_2 = 0$ the flow will closely follow $\Gamma = 0$ trajectories. If a trajectory approaches a periodic orbit above Q^* , the term Γa_1 in Eq.(9a) will make a_1 ultimately diverge, as the system slowly drifts through the set of periodic orbits; if the $\Gamma = 0$ trajectory approaches the arc $P_0^*Q^*$, the system will first have a_1 slowly rising along and very close to Λ , till reaching the set of periodic orbits at point Q^* . The case for $\Gamma = 0$ trajectories approaching either the arc QP_0 or the periodic orbits below is dramatically different.

Consider flow in the vicinity of the $\Gamma = 0$ heteroclinic orbit corresponding to a Λ -point M on the $P_0P_0^*$ arc, in the approach back to the surface $a_2 = 0$, below P_0 . If the orbit approaches some point m between Q and P_0 and because of the term Γa_1 , a_1 should eventually start growing at rate Γ , keeping close to Λ . In terms of the eigenvalue λ_3 of Sec. 3, Eq.(9b) can be written as $da_2/dt = \lambda_3 a_2$; since λ_3 is negative for Λ -points below P_0 and positive from P_0 to P_0^* , and the a_1 -rise takes times of order $1/\Gamma$, a_2 will become exponentially small ($-\ln a_2 \sim 1/\Gamma$). Once P_0 is reached, however, a_2 will start growing; when values $a_2 \sim \sqrt{\Gamma}$ are attained, a_1 can finally reach a maximum M' below P_0^* , and the trajectory again start separating from Λ . If the heteroclinic orbit approaches some periodic orbit below Q , a_1 will first slowly increase while the system drifts among the lower set of periodic orbits to reach Λ .

In the parametric domain of Fig.2 where P is stable, trajectories starting within some *bassin* of attraction in phase space have a sequence of points M, m, M', \dots , converging to point P as given, to lowest order in Γ , by Equations (14) and $a_2^2 = \Gamma \times a_1^2/\gamma$. The general

attractor structure following the loss of stability of P at crossing line B (or C) at fixed \bar{V} , giving rise to a limit cycle, depends on the value of \bar{V} . At \bar{V} very close to unity the set of periodic orbits is rarely involved in the attractor.

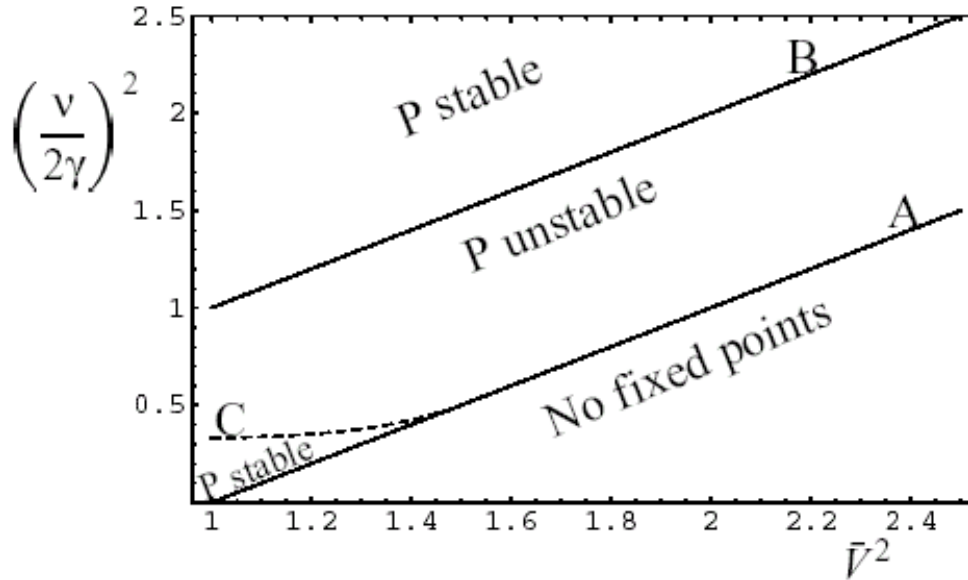


Figure 2. Stability of fixed point P at $\Gamma \rightarrow 0^+$, in parametric plane $(v/2\gamma)^2, \bar{V}^2$.
 Lines A, $(v/2\gamma)^2 = \bar{V}^2 - 1$; B, $(v/2\gamma)^2 = \bar{V}^2$; C, given by Eq.(19).

5. NUMERICAL RESULTS

In this section we study to cases: $\Gamma = 0$ and $\Gamma \rightarrow 0^+$ by means of numerical integration of the Equations (9a-c). The numerical integration is carry out by a single step, 8th order Runge-Kutta method.¹⁸

5.1 Case $\Gamma = 0$

We present two figures, one of them (Figure 3) shows the trajectory and long-time attractor (a periodic orbit) for $\bar{V} = 13/12$ ($k_3/k_2 = 4/9$), $\Gamma/\gamma = 0$ and $v/\gamma = 1.6$ with $\gamma = 1$, considering the initial conditions: $a_1 = 1.0$, $a_2 = 2.7$ and $\beta = 5$. One can observe that the trajectory converge asymptotically to a periodic orbit on $a_2 = 0$ plane below the point Q. Figure 4 shows the trajectory, curve Λ and long-time attractor (a periodic orbit) projected on the $a_1 - \beta$ plane for $\bar{V} = 13/12$ ($k_3/k_2 = 4/9$), $\Gamma/\gamma = 0$ and $v/\gamma = 1.6$ with $\gamma = 1$, considering as initial conditions $a_1 = 1.0287$, $a_2 = 0.0001$ and $\beta = 1.237$. The initial conditions represents a point placed on surface $h_0 = 0$ close to the arc $P_0P_0^*$ of the curve Λ . This point has an 1D unstable manifold transverse to $a_2 = 0$ plane; an heteroclinic orbit leaves this plane at this point, and return to it at a lower a_1 on periodic orbit.

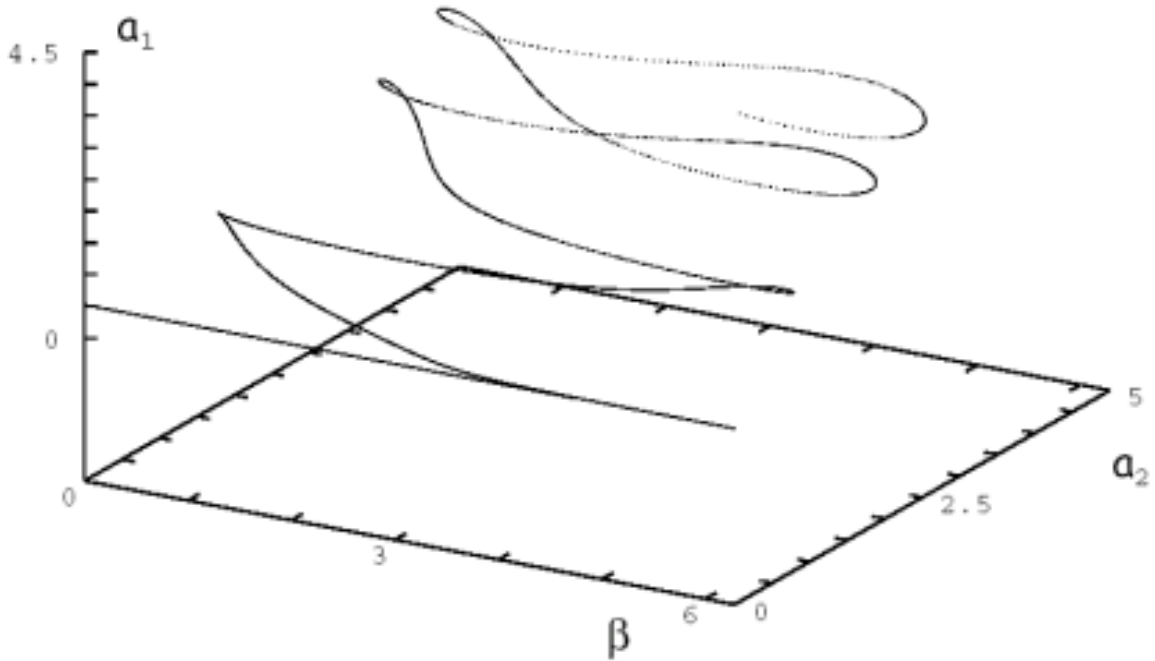


Figure 3. Trajectory and long-time attractor (a periodic orbit) for $\bar{V} = 13/12$ ($k_3/k_2 = 4/9$), $\Gamma/\gamma = 0$ and $v/\gamma = 1.6$ with $\gamma = 1$. Initial conditions: $a_1 = 1.0$, $a_2 = 2.7$ and $\beta = 5$.

5.2 Case $\Gamma \rightarrow 0^+$

To analyze the loss of stability of point P at crossing the lines B and C by fixed \bar{V} , we presents the results by $\bar{V} = 13/12$ ($k_3/k_2 = 4/9$) and $\Gamma/\gamma = 0.001$, with $\gamma = 1$. Line B corresponds to $v/\gamma = 2.166$ and line C to $v/\gamma = 1.16$, so that the unstable range is $1.16 \leq v/\gamma \leq 2.166$ (see Figure 2). Table 1 summarize the numerical results, it is possible to observe the evolution of the attractor structure in function of v/γ , using as initial conditions $a_1 = 2.0$, $a_2 = 0.1$ and $\beta = 2.0$. We found the Feigenbaum cascade to chaos: 1-limit-cycle, 2-limit-cycle, 4-limit-cycled and chaos. Figure 5 shows a 1-limit-cycle attractor, projected on the $a_1 - \beta$ plane, for $v/\gamma = 1.8$, which is determined following a single trajectory for long times. Figure 6 shows a 2-cycle-limit attractor by $v/\gamma = 1.60125$, Figure 7 shows a 4-cycle-limite attractor by $v/\gamma = 1.601203$ and Figure 8 represents the chaotic attractor by $v/\gamma = 1.6$.

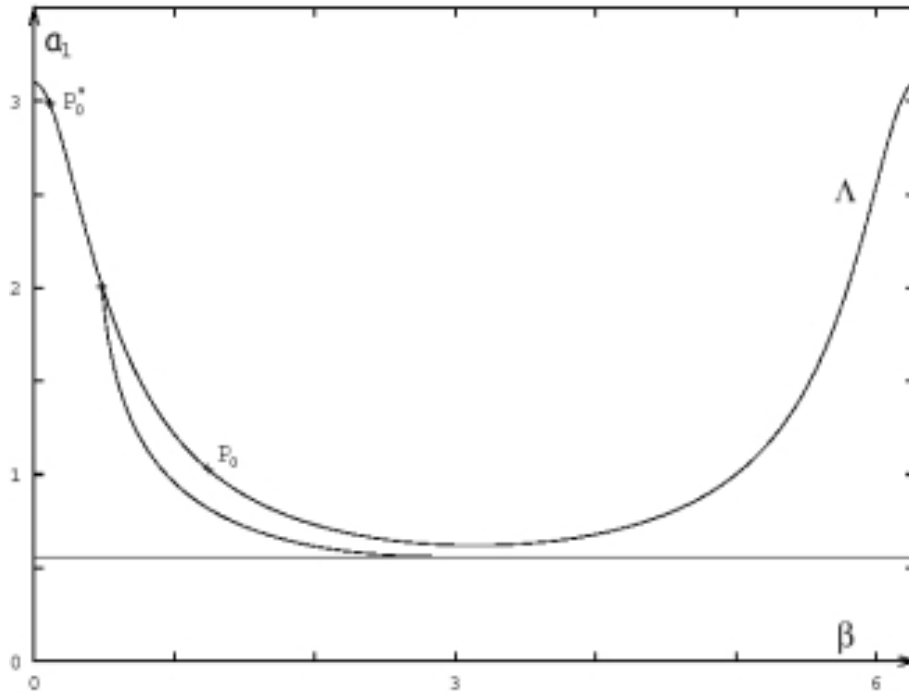


Figure 4. Trajectory, curve Λ and long-time attractor (a periodic orbit) for $\bar{V} = 13/12$ ($k_3/k_2 = 4/9$), $\Gamma/\gamma = 0$ and $v/\gamma = 1.6$ with $\gamma = 1$. Initial conditions: $a_1 = 1.0287$, $a_2 = 0.0001$ and $\beta = 1.237$.

v/γ	Δt	Time step number	Attractor structure
2.5	0.05	10150000	$\beta = 1.724165 - a_2 = 0.03181 - a_1 = 1.00592$
2.2	0.05	40200000	$\beta = 1.587941 - a_2 = 0.031625 - a_1 = 1.000073$
2.1	0.005	101600000	1-limit-cycle
2.0	0.05	40200000	1-limit-cycle ascending by periodic orbits
1.8	0.05	40200000	1-limit-cycle ascending by periodic orbits
1.7	0.05	40200000	1-limit-cycle ascending by periodic orbits
1.65	0.05	40200000	1-limit-cycle ascending by periodic orbits
1.64	0.005	51600000	1-limit-cycle ascending by periodic orbits
1.61	0.05	40200000	1-limit-cycle ascending by periodic orbits
1.602	0.005	101200000	1-limit-cycle ascending by periodic orbits
1.60125	0.005	51200000	2-limit-cycle ascending by periodic orbits
1.601203	0.005	41200000	4-limit-cycle ascending by periodic orbits
1.6	0.005	101600000	Chaos
1.58	0.05	20200000	1-limit-cycle ascending by periodic orbits
1.5	0.05	40200000	1-limit-cycle
1.4	0.05	40200000	1-limit-cycle
1.2	0.05	40200000	1-limit-cycle
1.0	0.05	40200000	$\beta = 0.712956 - a_2 = 0.039101 - a_1 = 1.23648$

Table 1. Numerical results by $\bar{V} = 13/12$ ($k_3/k_2 = 4/9$) and $\Gamma/\gamma = 0.001$, with $\gamma = 1$. Initial conditions: $a_1 = 2.0$, $a_2 = 0.1$ and $\beta = 2.0$

VI. CONCLUSIONS

We have truncated the derivative nonlinear Schrödinger (DNLS) equation describing the interaction of circularly polarized Alfvén waves of finite amplitude, to explore weakly nonlinear dynamics in the coherent cubic coupling of three waves near resonance (3WRI), wave 1 being linearly unstable and waves 2 and 3 damped. We have considered a broad scenario for chaos which several 3WRI systems had exhibited: No matter how small the growth rate Γ of the unstable wave there exists certain parametric domain with a fully developed attractor (chaotic in some subdomain) that is absent at $\Gamma \leq 0$. To explore the characteristics of this hard transition to complex phase-space dynamics we have considered a *reduced* 3-wave model (equal dampings of daughter waves, leading to a 3D flow for wave amplitudes a_1 , a_2 and a relative phase).

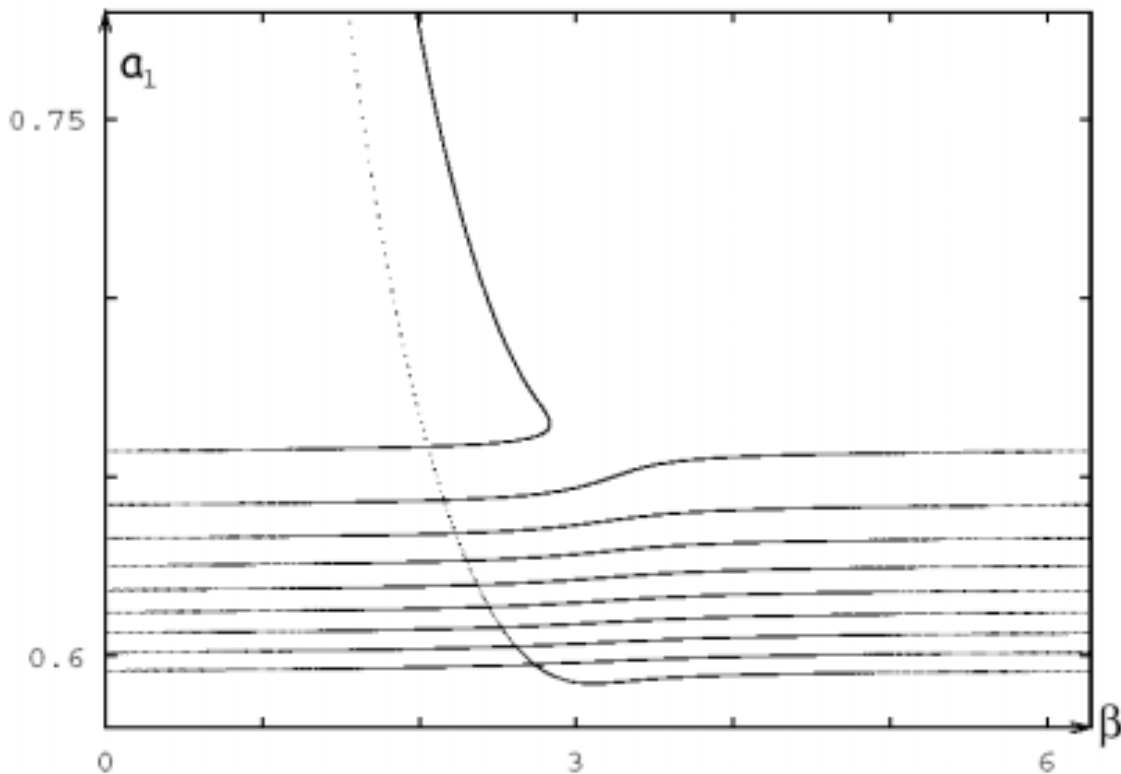


Figure 5. Lower part of limit 1-cycle attractor projected on the $a_1 - \beta$ plane for $\bar{V} = 13/12$ ($k_3/k_2 = 4/9$), $\Gamma/\gamma = 0.001$ and $\nu/\gamma = 1.8$ with $\gamma = 1$.

The reduced model showed the hard transition only occurring for left-hand circularly polarized waves, paralleling the known fact that LH time-harmonic solutions of the DNLS equation (for cold plasmas) are modulationally unstable, a case opposite RH polarized solutions.⁵ A number of features determine the phase-space dynamics of the transition: For $\Gamma = 0$, the entire flow is asymptotic to the space $a_2 = 0$, where a line of fixed points Λ covers

a limited a_1 -range with periodic orbits below and above that range. A branch of Λ has an arc of fixed points unstable off the space $a_2 = 0$, in between stable arcs; singular, heteroclinic orbits off the unstable arc return to that space at lower a_1 . Chaotic attractors involve repeated slow rises on Λ , and possibly in the lower set of periodic orbits, followed by fast motion along the heteroclinic orbits.

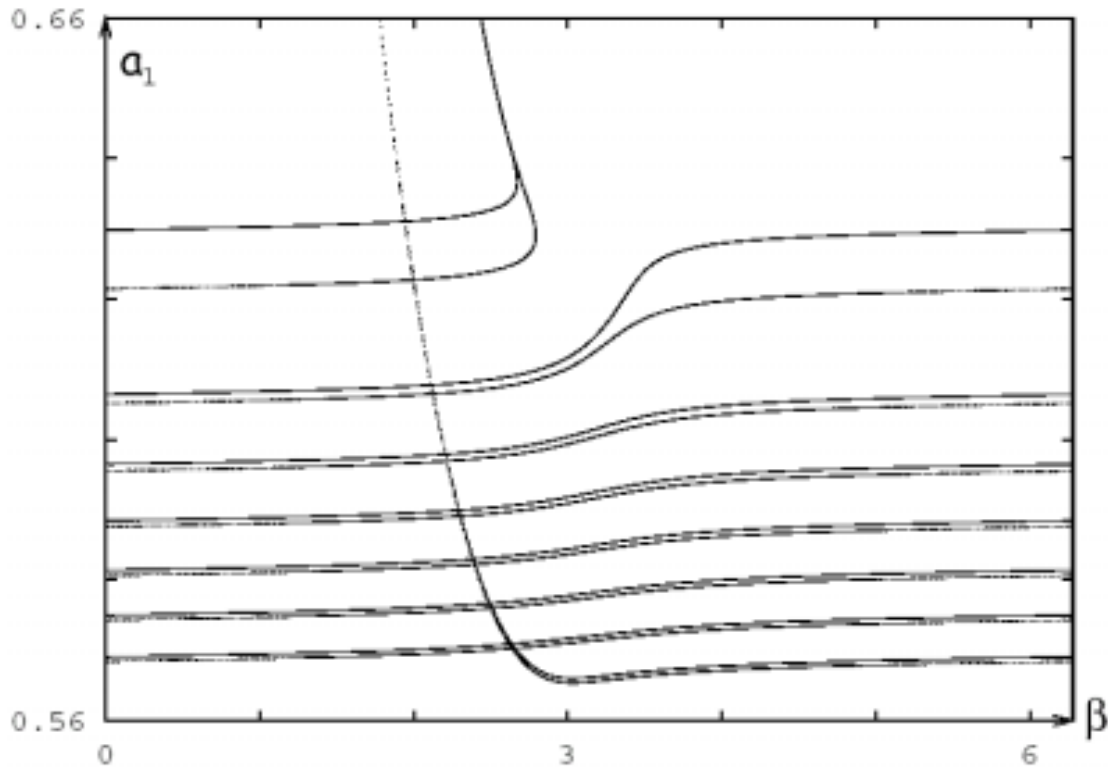


Figure 6. Lower part of limit 2-cycle attractor projected on the $a_1 - \beta$ plane for $\bar{V} = 13/12$ ($k_3/k_2 = 4/9$), $\Gamma/\gamma = 0.001$ and $\nu/\gamma = 1.60125$ with $\gamma = 1$.

Acknowledgments

This work was supported by Ministerio de Ciencia y Tecnología of Spain, under Grant BFM01-3723, Secretaría de Ciencia y Tecnología of Universidad Nacional de Córdoba and Agencia Córdoba Ciencia. Work by S. Elaskar was, partially, supported by Ministerio de Educación Cultura y Deportes of Spain, under Grant SB01-0080.

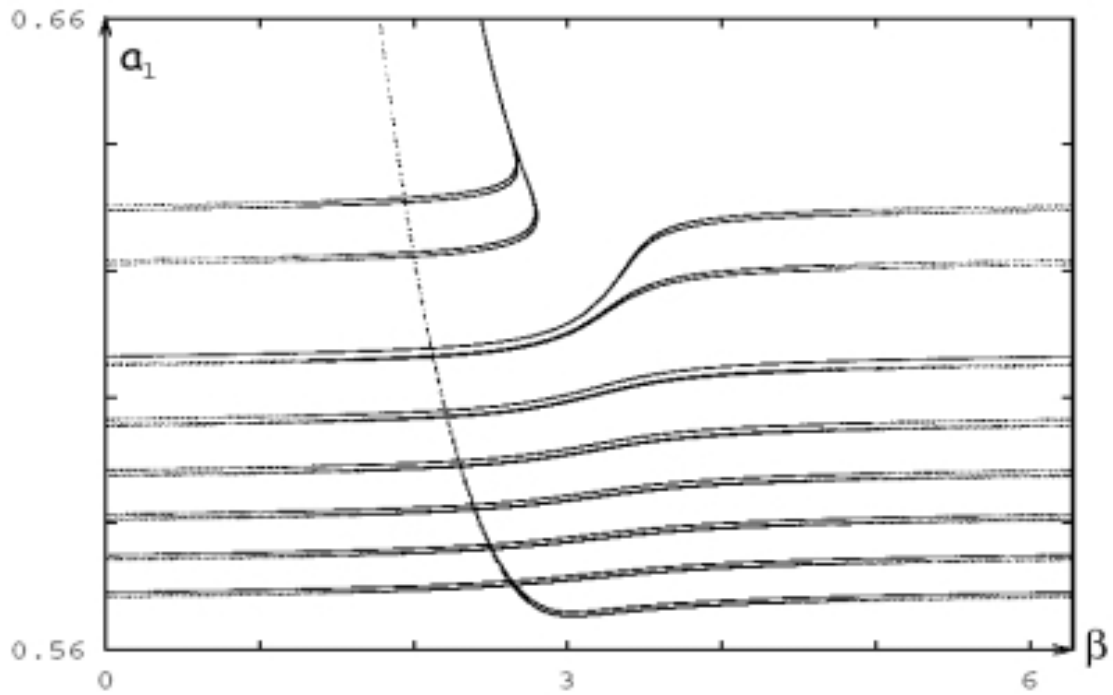


Figure 7. Lower part of limit 4-cycle attractor projected on the $a_1 - \beta$ plane for $\bar{V} = 13/12$ ($k_3/k_2 = 4/9$), $\Gamma/\gamma = 0.001$ and $\nu/\gamma = 1.601203$ with $\gamma = 1$.

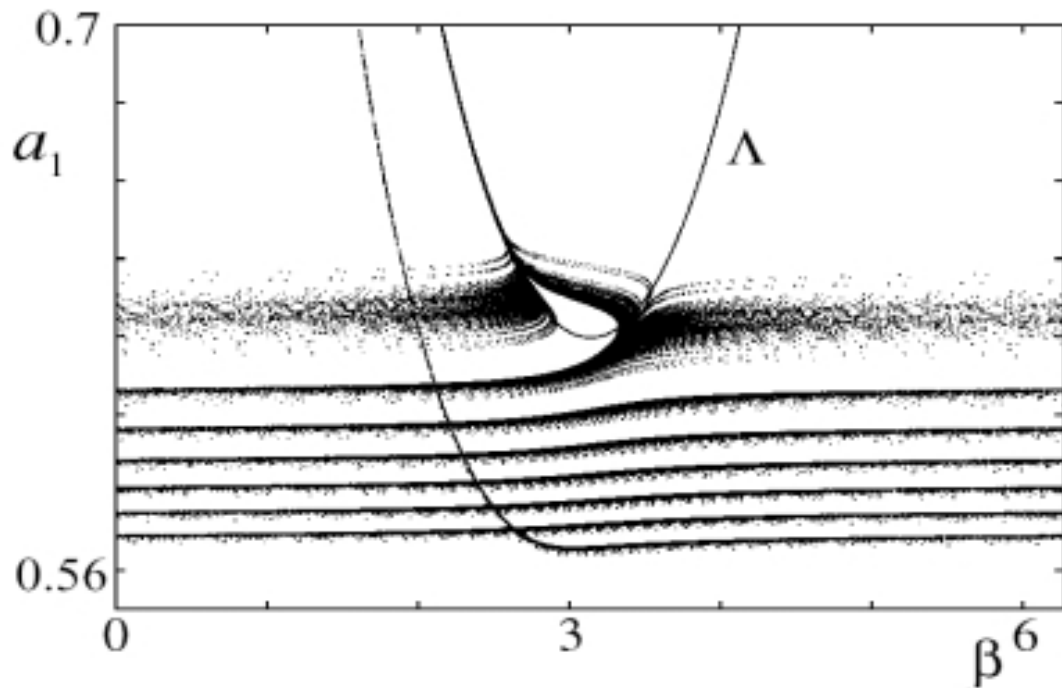


Figure 8. Lower part of chaotic attractor projected on the $a_1 - \beta$ plane, for $\bar{V} = 13/12$ ($k_3/k_2 = 4/9$), $\Gamma/\gamma = 0.001$, $\nu/\gamma = 1.6$ and $\gamma = 1$.

References

1. S.D.Drell, H.M.Foley and M.A.Ruderman, *J. Geophys. Res.* **70**, 3131 (1965); A.Barnett and S.Olbert, *J. Geophys. Res.* **91**, 10117 (1986); J.R.Sanmartín and M.Martínez-Sanchez, *J. Geophys. Res.* **100**, 1677 (1995).
2. J.R.Sanmartín and R.D.Estes, *J. Geophys. Res.* **102**, 14625 (1997).
3. G.V.Khazanov, N.H.Stone, E.N.Krivorutsky and E.W.Liemohn, *J. Geophys. Res.* **105**, 15835 (2000); G.V.Khazanov, N.H.Stone, E.N.Krivorutsky, K.V.Gamayunov and E.W.Liemohn, *J. Geophys. Res.* **106**, 10565 (2001); J.R.Sanmartín and R.D.Estes, *J. Geophys. Res.* **107**, SIA 2-1 (2002).
4. A.Rogister, *Phys. Fluids* **14**, 2733 (1971); K.Mio, T.Ogino, K.Minami and S.Takeda, *J. Phys. Soc. Japan* **41**, 265 (1976).
5. E.Mjølhus, *J. Plasma Phys.* **16**, 321 (1976); **19**, 437 (1978).
6. S.R.Spangler and J.P.Sheerin, *J. Plasma Phys.* **27**, 193 (1982); T.Hada, C.F.Kennel and B.Butl, *J.Geophys. Research* **94**, 65 (1989); M.V.Medvedev and P.H.Diamond, *Phys. Plasmas* **3**, 863 (1996); T.Passot and P.L.Sulem, *Phys. Plasmas* **10**, 3887 (2003).
7. R.C.Davidson, *Methods in Nonlinear Plasma Theory* (Academic, New York, 1972), Chap. 6; A. Bers, in *Plasma Physics - Les Houches 1972*, edited by C.De Witt and J.Peyreud (Gordon and Breach, New York, 1975), pp. 117-215; J.Weiland and H.Wilhelmsson, *Coherent Nonlinear Interaction of Waves and Plasmas* (Pergamon, New York, 1977).
8. S.Ya.Vyshkind and M.I.Rabinovich, *Sov.Phys.-JETP* **44** 292 (1976); A.S.Pikovsky and M.I.Rabinovich, *Physica D* **2**, 8 (1981).
9. J.M.Wersinger, J.M.Finn, and E.Ott, *Phys.Rev.Lett.* **44**, 453 (1980); *Phys.Fluids* **23**, 1142 (1980).
10. M.N.Bussac, *Phys.Rev.Lett.* **49**, 1939 (1982); C.Meunier, M.N.Bussac and G.Laval, *Physica D* **4**, 236 (1982).
11. D.W.Hughes and M.R.E.Proctor, *Physica D* **46**, 163 (1990).
12. O.López-Rebollal and J.R.Sanmartín, *Physica D* **89**, 204 (1995).
13. D.W.Hughes and M.R.E.Proctor, *Wave Motion* **20**, 201 (1994).
14. O.López-Rebollal, J.R.Sanmartín and E. del Río, *Phys. Plasmas* **5**, 2861 (1998).
15. M.I.Rabinovich and A.L.Fabrikant, *Sov. Phys. JETP* **50**, 311 (1979); D.A.Russell and E.Ott, *Phys. Fluids* **24**, 1976 (1981).
16. J.R.Sanmartín, O.López-Rebollal, and N.de Paola, *Physica D* **69**, 148 (1993).
17. J.R.Sanmartín, O.López-Rebollal, and E. Del Río; S. Elaskar, *Physics of Plasmas* **11**, 2026 (2004).
18. E. B. Shanks, *Math. Comp.* **20**, 21-38 (1966)